ARMY RESEARCH LABORATORY

A Three-Dimensional Foil Bearing Performance Map Applied to Oil-Free Turbomachinery

by Kevin C. Radil and Christopher DellaCorte

ARL-TR-4473   **April 2009**

NOTICES

Disclaimers

The findings in this report are not to be construed as an official Department of the Army position unless so designated by other authorized documents.

Citation of manufacturer's or trade names does not constitute an official endorsement or approval of the use thereof.

Destroy this report when it is no longer needed. Do not return it to the originator.

Army Research Laboratory

NASA-Glenn Research Center, Cleveland, OH 44135-3191

ARL-TR-4473   April 2009

A Three-Dimensional Foil Bearing Performance Map Applied to Oil-Free Turbomachinery

Kevin C. Radil
Vehicle Technology Directorate, NASA-Glenn Research Center, ARL

and

Christopher DellaCorte
NASA-Glenn Research Center, Cleveland, OH

REPORT DOCUMENTATION PAGE				*Form Approved* *OMB No. 0704-0188*
Public reporting burden for this collection of information is estimated to average 1 hour per response, including the time for reviewing instructions, searching existing data sources, gathering and maintaining the data needed, and completing and reviewing the collection information. Send comments regarding this burden estimate or any other aspect of this collection of information, including suggestions for reducing the burden, to Department of Defense, Washington Headquarters Services, Directorate for Information Operations and Reports (0704-0188), 1215 Jefferson Davis Highway, Suite 1204, Arlington, VA 22202-4302. Respondents should be aware that notwithstanding any other provision of law, no person shall be subject to any penalty for failing to comply with a collection of information if it does not display a currently valid OMB control number. **PLEASE DO NOT RETURN YOUR FORM TO THE ABOVE ADDRESS.**				

1. REPORT DATE *(DD-MM-YYYY)*	2. REPORT TYPE	3. DATES COVERED (From - To)
April 2009	Final	January to August 2007

4. TITLE AND SUBTITLE	5a. CONTRACT NUMBER
A Three-Dimensional Foil Bearing Performance Map Applied to Oil-Free Turbomachinery	
	5b. GRANT NUMBER
	5c. PROGRAM ELEMENT NUMBER
6. AUTHOR(S)	5d. PROJECT NUMBER
Kevin C. Radil (ARL) and Christopher DellaCorte (NASA-Glenn)	
	5e. TASK NUMBER
	5f. WORK UNIT NUMBER

7. PERFORMING ORGANIZATION NAME(S) AND ADDRESS(ES)	8. PERFORMING ORGANIZATION REPORT NUMBER
U.S. Army Research Laboratory ATTN: AMSRD-ARL-VT-PD John H. Glenn Research Center at Lewis Field Cleveland, OH 44135-3191	ARL-TR-4473

9. SPONSORING/MONITORING AGENCY NAME(S) AND ADDRESS(ES)	10. SPONSOR/MONITOR'S ACRONYM(S)
	11. SPONSOR/MONITOR'S REPORT NUMBER(S)

12. DISTRIBUTION/AVAILABILITY STATEMENT

Approved for public release; distribution unlimited.

13. SUPPLEMENTARY NOTES

14. ABSTRACT

To effectively apply compliant foil gas bearings to increasingly larger and more challenging turbomachinery, a comprehensive method that compares a foil bearing's capabilities with the application's operating requirements is needed. Extensive laboratory and field experience suggests foil bearing failure is generally due to thermal stress brought on by excessive viscous power loss; therefore a map that graphically relates component and system-level parameters (bearing size, applied loads, and shaft rotational speeds) directly to bearing power loss is more elucidating than a map based on a lumped speed/load parameter like the Sommerfeld number. In this report we describe a performance map featuring a three-dimensional contour plot that illustrates the expected power loss in a foil bearing as a function of applied load and shaft speed. Using this performance map, bearing capabilities can be examined at the anticipated system operating conditions and safety margins between an operating point and incipient bearing failure can be ascertained. To demonstrate the concept's features and usefulness, we present a performance map generated from foil bearing power loss test data. We expect these maps, combined with other predictive tools, will help evaluate a foil bearing's general suitability for a candidate rotor system and will lead to more robust and successful Oil-Free turbomachinery designs.

15. SUBJECT TERMS

Foil bearing, gas bearing, turbomachinery

16. SECURITY CLASSIFICATION OF:			17. LIMITATION OF ABSTRACT	18. NUMBER OF PAGES	19a. NAME OF RESPONSIBLE PERSON Kevin Radil
a. REPORT	b. ABSTRACT	c. THIS PAGE	UU	22	19b. TELEPHONE NUMBER (*Include area code*)
Unclassified	Unclassified	Unclassified			(216) 433-5047

Contents

List of Figures

List of Tables

1. Introduction

Foil bearings are self-acting, hydrodynamic gas bearings that use air as their working fluid. Their use in rotating systems eliminates the weight, maintenance requirements, speed, and temperature limitations associated with conventional oil-lubricated rotor supports (i.e., bearings, dampers, seals and oil-system) (*1–3*). Gas foil bearing technology has been deployed in many high-speed rotating shaft systems such as air cycle machines, turboexpanders, and compressors and in small micro-turbine systems (*4–6*). Additionally, foil bearings have been demonstrated as "proof-of-concepts" in diesel engine turbochargers, auxiliary power units (APUs), and selected hot section bearings in gas turbines (*7–9*). While these Oil-Free turbomachines represent the successful final outcomes of foil bearing integration efforts, most were achieved through arduous "make and break" hardware-intensive development programs. This inefficient approach is often employed because, despite foil bearings' long use, little effort has been undertaken to develop a systematic approach to streamline their integration into new, high-speed turbomachinery systems.

Figure 1 shows a cross section of a radial foil air bearing. This type of fluid-film gas bearing employs a series of thin sheet metal foils, from which its name is derived. The foils are typically made from a nickel-based superalloy, because this material retains a majority of its elastic spring properties at high temperatures. Bearing construction is based on three main components: the top foil, the bump foil, and the shaft. The top foil acts as a compliant surface that traps and supports the hydrodynamic gas film against the rotating shaft. It rests on a corrugated foil layer, known as the bump foil, which serves as an elastic spring foundation that provides the bearing its compliancy. As the shaft rotates, it pumps air into the hydrodynamic gas film via a viscous dragging mechanism. Consequently, the generated gas film pressure, and therefore resulting bearing performance, is directly proportional to speed. During start-up, shut-down, and periods of very low shaft speed, there is an insufficient lubricating gas film to maintain separation and sliding contact occurs between the top foil and the shaft. To address these contact episodes, solid lubricants are applied to the top foil and/or shaft to reduce friction and minimize wear.
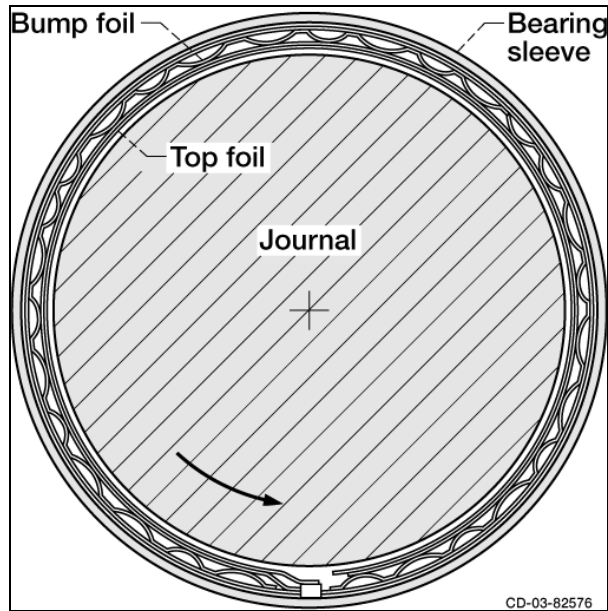
Figure 1. Cross-sectional view of a radial foil air bearing.

Recently, we have been advocating a four-step process designed to guide the development of foil air bearing supported turbomachinery and reduce risk. The four steps include (1) a rotordynamic feasibility and layout trade study, (2) bearing sizing and testing, (3) experimental rotordynamic simulator validation tests, and (4) a system-level demonstration. The first two steps contain component and system-level experimental work supplemented by various analytical and empirical modeling tools. For instance, the rotordynamic feasibility step combines computer-based, finite element rotordynamic modeling with empirical equations regarding load capacity and stiffness and damping characteristics to predict the stability of a proposed shaft design in the form of a critical speed map. The bearing sizing effort in step two encompasses experimental verification of the bearing's load capacity to ensure that its size is adequate for the application. The last two steps focus on the overall system by demonstrating operation first on a rotor simulator to uncover any unforeseen integration problems requiring attention followed by the system-level demonstration. Even though the four-step process is a viable developmental approach, there are still missing elements that challenge our ability to predict system-level foil bearing performance.

For example, one such poorly understood aspect of foil bearing performance recently identified is thermal management and stability (*10, 11*). Depending on the speed, foil bearings generate a moderate amount of heat due to viscous shearing of the thin gas film. If left unchecked, build-up of this heat can cause localized hotspots, resulting in excessive thermal gradients and possible bearing seizure. The most common approach to removing this heat is to flow an adequate amount of air axially behind the top foil and through the bearing's bump foils. Another effective method (*10*) is to impinge a jet of air directly on the inner surface of a hollow rotating shaft coincident with the bearing, thereby turning the shaft into a rotating heat exchanger for the

2

gas film. Regardless of the strategy, research suggests proper thermal management is a key fundamental necessity for the successful deployment and operation of foil bearings in high-speed turbomachinery systems.

To address the lack of system-level design tools, we introduced the concept of a performance map for foil air bearings. This map is a plot of bearing power loss versus speed covering start-up to high-speed operation and describes bearing operating regimes, performance safety margins, and the effects of load. The map, as seen in figure 2 from reference 12, is for a constant applied load and resembles a Stribeck curve for bearing friction. It is divided into two distinct operating regimes, designated as the highly loaded, thin-film regime and the lightly loaded, viscosity-dominated regime. The minimum in the curve represents the instance where a sufficiently thick gas film develops to support the load, but the speed is still low to prevent excessive viscous losses. The area to the left of this minimum point is the high load region and is where the bearing's power loss is dominated by the thin-film shear occurring in the high-pressure, load support zone. A foil bearing operating in this region will experience large fluctuations in its power loss in response to very small changes to speed and/or load and is susceptible to a failure mechanism known as thermal runaway.
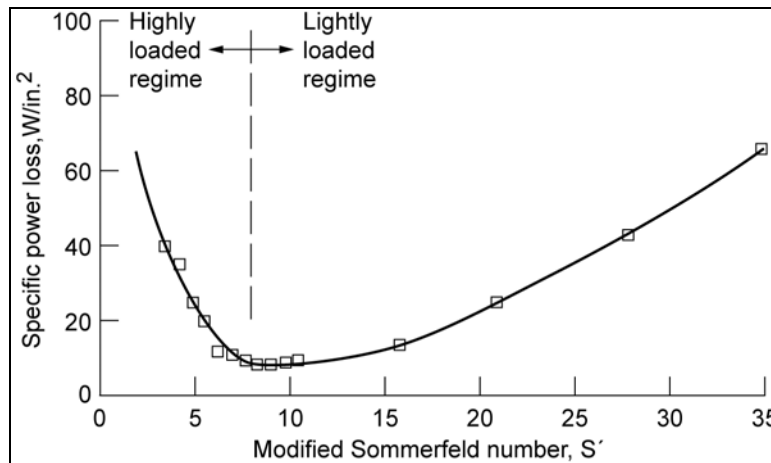

Figure 2. Foil bearing performance map (*12*) illustrating its general shape
and the two operating regions.

Thermal runaway is a consequence of the thermal growth mismatch between the shaft and bearing and manifests as a continual increase in preload. During operation, most of the viscous heat generated in the gas film is conducted into the shaft and bearing (*13*). However, the small cross section of the bump foils limits the rate of heat conduction to the surrounding structure, effectively isolating the thin top foil. This causes the top foil to quickly reach the temperature of the adjacent gas film leaving the shaft to absorb most of the continuous supply of viscous energy. As the shaft expands, it squeezes the air film uniformly around the bearing's circumference, which mimics an increase in preload and expends available load capacity. This extra load on the bearing produces additional heating and further growth of the shaft, thereby beginning a thermal

repetitive cycle that will eventually overload the bearing and cause seizure. Understandably, bearings designed with an initially high preload for proper stiffness and damping properties are more susceptible to this type of failure mechanism.

Alternately, the area to the right of the load curve's minimum has been termed as the low load region and is characterized by a more thermally stable operating point for the bearing. In this region the entire circumference of the bearing contributes to the power loss via a windage mechanism instead of from localized viscous shear in the high pressure zone. However, the high speeds in this region can cause the thermal gradients to grow to dangerous levels that will result in bearing failure unless an adequate thermal management strategy is employed.

Despite its importance to Oil-Free systems, little appears to be publicly known regarding assessing the thermal robustness of a foil bearing application. Put another way, there is no clear and accepted method to judge how much performance margin exists for a foil bearing with respect to system-level parameters such as shaft speed, load, and thermal stability. This report addresses this shortfall by proposing a three-dimensional (3-D) map that parametrically and experimentally characterizes foil bearing power loss as a function of operating speed and load and provides a measurable margin of safety for an anticipated application.

2. Methods, Assumptions, and Procedures

2.1 Foil Bearing and Journal

The test bearing used to demonstrate the concept of a 3-D performance map is a Generation III version of the bearing shown in figure 1. Generation III is a category label for foil bearings with improved performance in both load capacity and stiffness and damping properties due to a spatially varying support structure in the circumferential, axial, and/or radial directions (*14*). The test bearing was nominally 35 mm in diameter, 27 mm long, and weighed 1.42 N.

The mating test journal was prepared by first plasma spraying PS304, a high temperature solid lubricant coating, onto the surface then placing it into a 540 °C oven for 100 h (*15*). After the heat treatment process, the journal was affixed to the test rig and machined with an in-place grinding system to the nominal final diameter of 35 mm, resulting in a bearing preload of 7.1 kPa. Finally, a computer program, based on the two-plane influence coefficient method, was used to balance the rig to 55 krpm.

Figure 3 shows the testing we performed on the high-speed rig. The rig consists of a drive shaft in an overhung configuration supported on ceramic, hybrid ball bearings that are lubricated by a closed-loop oil system. Rig bulk temperatures are controlled by circulating chilled water through the housing. An air impulse turbine attached to the main shaft is capable of driving the journal to a maximum rotational speed up to 60 krpm. The rod extending from the ring stack acts as a

moment arm to relay the bearing's operating torque to a load cell for power loss calculations. To effectively unload the bearing during startup and shutdown, a pulley-cable system using a pneumatic cylinder was installed to suspend the stack. A scatter shield placed around the bearing provided a safe operating environment (*16*).
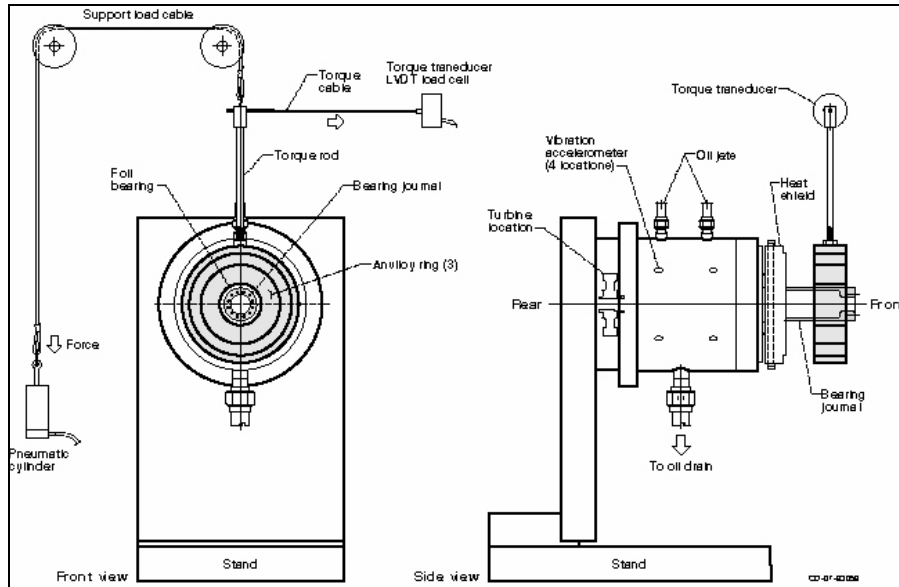

Figure 3. Foil bearing high-speed test rig with a stack of three Anviloy rings in place.

Since the PS304 coating in an as-ground condition will undergo break-in during initial operation, the test bearing and journal were together subjected to approximately 1500 start-stop cycles at 540 °C to eliminate this effect from influencing the data. The start-stop cycles act as a polishing wear mechanism between the asperities of the top foil and coating, resulting in a smooth, glossy, oxide surface on the PS304 coating and the development of a solid lubricant layer on the foil surface (*17*). After the break-in cycles, the final coating surface roughness was approximately 0.2 μm.

To obtain accurate power loss measurements, four dead weights in the form of rings made from Anviloy, a heavy tungsten alloy, were fabricated to apply radial loads to the bearing. Each ring weighed about 44 N and was sized so that they could be stacked to simulate loads of 44, 88, 132, and 176 N (figure 4). Holes in the rings provided access for the torque rod to be screwed into the innermost ring to hold the stack in place. Metal shims placed in the small space between the rings centered the weight assembly with respect to the bearing to facilitate single plane static balancing of the stack. Because of size differences, the test bearing had to be first placed in a steel ring that weighed 21.4 N and secured before inserting into the innermost Anviloy ring when higher radial loads were required.

Figure 4. Exploded view of Anviloy rings capable of producing
bearing loads from approximately 44 to 176 N. (Steel
housing for 35 mm bearing not shown).

The power loss tests were conducted at room temperature to provide a known constant ambient
environment. The first test began by inserting the bearing into the steel ring and securing it with
a set screw. The bearing assembly was then placed on the journal, the torque cable attached to
the load cell and the load support cable hooked to the torque rod. The test load, which included
the bearing weight and steel ring, was 23 N. To provide a more thermally stable system, a guide
tube was positioned to inject 0.20 m^3/min cooling air into the journal after placement of the
scatter shield. This is known as the indirect journal cooling method and is further described in
reference 10. Testing began by supporting the stack assembly with the pneumatic loader and
accelerating the journal to about 25 krpm to guarantee lift-off. The speed was then reduced and
held at a constant speed of approximately 20 krpm while the load cable was manually removed
from the torque rod to allow the bearing to freely support the weight. With the bearing floating
on the journal, the speed was dropped to the lowest attainable speed for the given stack weight
(determined through earlier tests) that would put operation in the high load region. Collection of
torque data began at this point and continued for each increment in speed according to the test
plan shown in table 1 until reaching 55 krpm. After recording the last data point, the speed was
dropped back to 20 krpm and the load cable reattached to the torque rod in preparation for rig
shutdown. The bearing-stack assembly was then suspended with the pneumatic loader while the
journal came to a complete stop. Once cool the stack was removed from the journal, a ring was
added, and the stack was balanced and then reinstalled on the rig. This test preparation and
operation was repeated for loads of 66 N and 109 N. Because of high ball bearing defect
frequencies in the rig, radial loads greater than 109 N were not attempted.

Table 1. Test speed increments for data collection.

Speed Range (rpm)	Speed Increments (rpm)
Up to 20,000	1000
20–30,000	2000
30–55,000	5000

2.2 Results and Discussion

Figure 5 shows the concept of a 3-D performance map for the test bearing, which was constructed with the power loss data collected at three different radial loads. The map has speed on the *x*-axis, power loss on the *y*-axis, and load on the *z*-axis. Presenting the data in a contour plot format not only quantifies the bearing's resulting power loss under steady-state conditions but also demonstrates its response to changes in both speed and load. As shown in the graph, as the bearing's radial load increased, the curves moved up and to the right. It is expected that additional load curves representing heavier loads will continue to shift up and to the right following the current trend. Each curve has a minimum that separates the low load and high load regimes and is the reference point for the concept of a margin of safety. The definition of a margin of safety is only relevant for a bearing operating in the low load region and is a measure of how much of a speed reduction can be tolerated before moving into the high load region. At this time, there is no set rule-of-thumb for how large the margin should be. It depends on the bearing's application, variations in the operating conditions, and the experience of the designer.
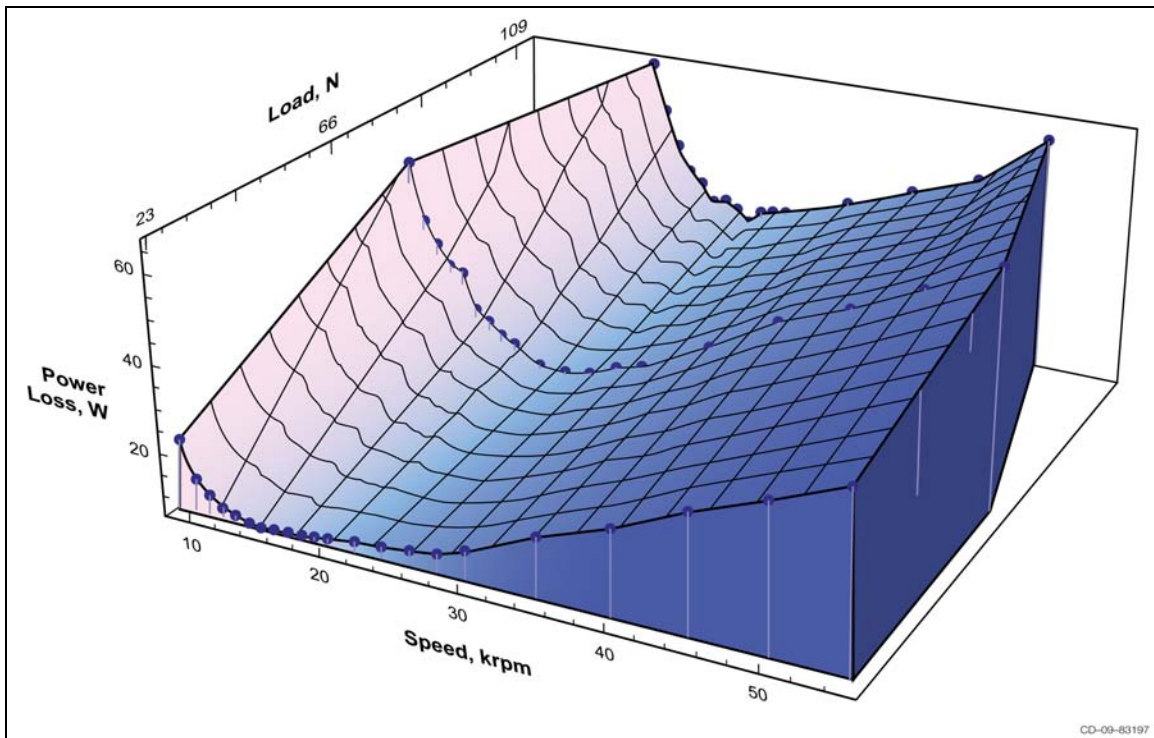

Figure 5. A 3-D performance map for the 35 mm diameter foil bearing generated from three load curves.

The usefulness and simplicity of the performance maps as a design tool can also be elucidated by presenting the test data in figure 5 on a two-dimensional (2-D) graph, as shown in figure 6, with power loss as a function of speed for different radial loads. This more user-friendly format enables the designer to directly predict the bearing's behavior throughout its expected operating envelope and also the margins of safety with respect to the high load region and then ascertain if the bearing's abilities are adequate to manage the system's speed and load requirements. To demonstrate, refer to the representative performance map in figure 7. If a system requires the bearing to idle at point A and withstand the maximum maneuver load conditions at B at full speed, the performance map indicates the bearing is thermally stable at idle since point A lies in the bearing's low load region and has a modest margin of safety. However, as the conditions change from A to B, the increase in speed and load causes the bearing's operating point to travel vertically up and to the right from one load curve to another until finally stopping at point B, which is an unstable condition that puts the bearing at risk of failure due to thermal runaway. If, for example, the bearing was allowed to operate at B and thermal runaway did manifest, the increase in preload force would most likely force a decrease in speed. This reaction would be represented on the map as point B traveling up and to the left from one load curve to another, moving deeper into the high load region, eventually ending in failure. A much more stable application for this size bearing would be in a system with higher operating speeds (or lower loads), where the idle condition was again at A but the maximum load condition was at point C, since both A and C remain in the low load region and have acceptable margins of safety to accommodate unforeseen fluctuations in system operating speed.
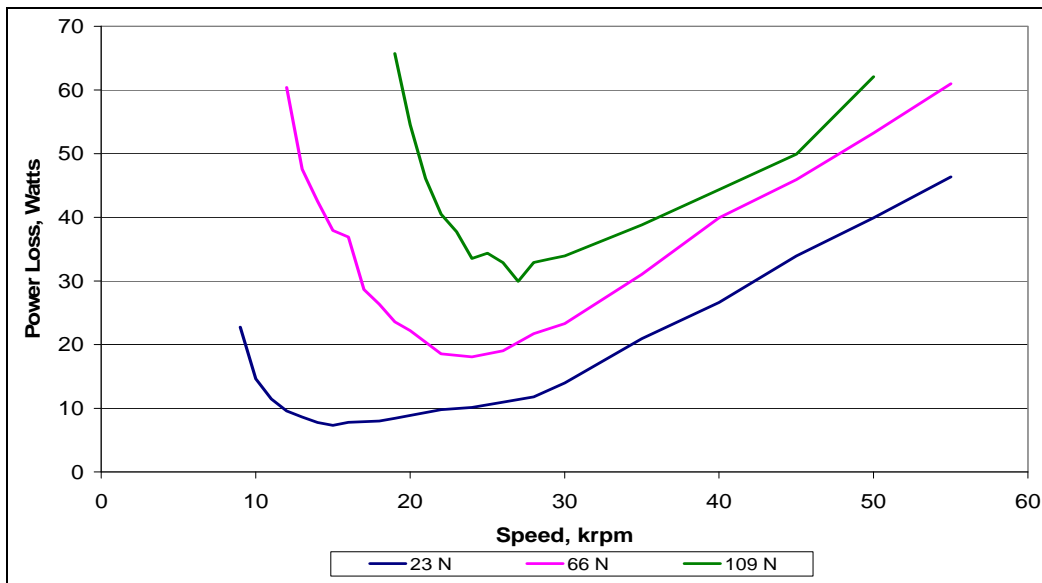

Figure 6. A 2-D performance map for the 35 mm diameter foil bearing using the three load curves.
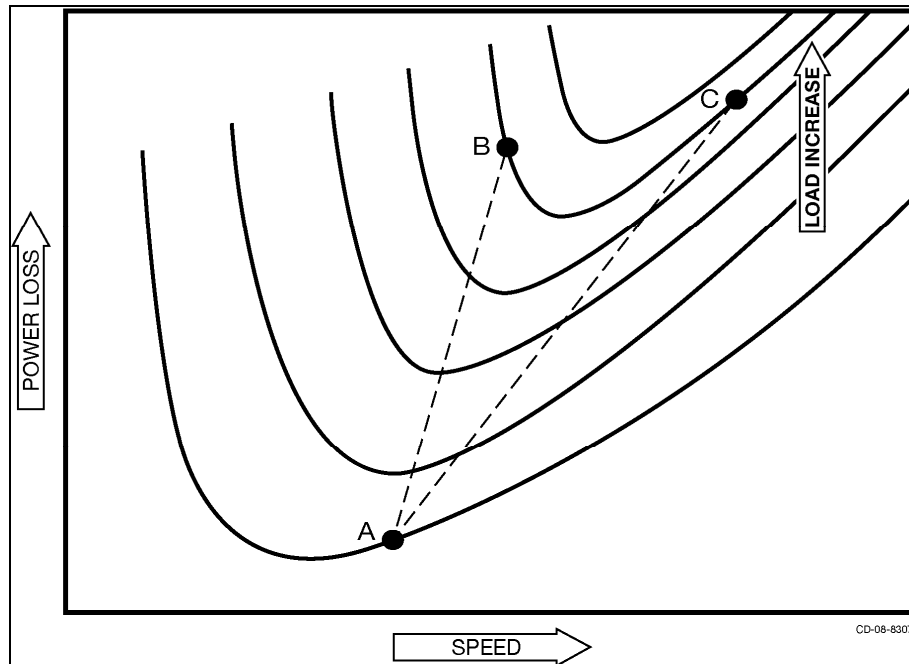
8

Figure 7. Representative performance map showing hypothetical operating points.
Operating points A and C are in the low load region and point B is in the high
load region.

Performance maps for other foil bearings types (overlapping leaf, multiple top foils), support
complexity (backing springs, multiple bump layers), and size are expected to exhibit the same
general behavior since they all rely on the principle of hydrodynamics but will vary according to
their own design characteristics. For example, the effect of bearing size on power loss was
studied by testing the bearing in figure 8, which was of similar design to the 35 mm bearing but
larger. This bearing's inner diameter and length were nominally 51 mm and had a type K
thermocouple tack welded to the middle of the spacer block and positioned just below the plane
of the top foil near the leading edge to monitor the bearing's internal temperature. Bearing
preload was not measured but is estimated to fall in the range of 6.9 to 10.3 kPa. The bearing
weighed 4.4 N and did not require a steel spacer to properly fit in the smallest Anviloy ring. To
address the ball defect frequencies the rig was rebuilt with new ball bearings. We only tested
radial loads of 48 N and 179 N, and followed the same test set-up and procedure, except thermal
management was administered by directly cooling the journal (*10*). As can be seen in figure 9,
the resulting 2-D plot does not show a huge difference between load curves, indicating that
heavier weights are needed for this size bearing to generate a more informative performance
map. Unfortunately, high synchronous vibrations prohibited testing loads greater than 178 N.
Even so, comparing the maps in figure 6 and 9 at identical speeds and applied load conditions
shows that the power loss signature generated by the 35-mm bearing is lower due to the smaller
top foil surface area. Consequentially, operating efficiency can be maximized by using the
smallest bearing that both satisfies the system's performance requirements and also has an
acceptable margin of safety. This information can be obtained by constructing maps for each foil

9

air bearings being considered for a high speed application. Bearing temperatures for selected operating points in figure 9 are provided in table 2 as reference data for the validation of future predictive computer models for advanced foil air bearings.
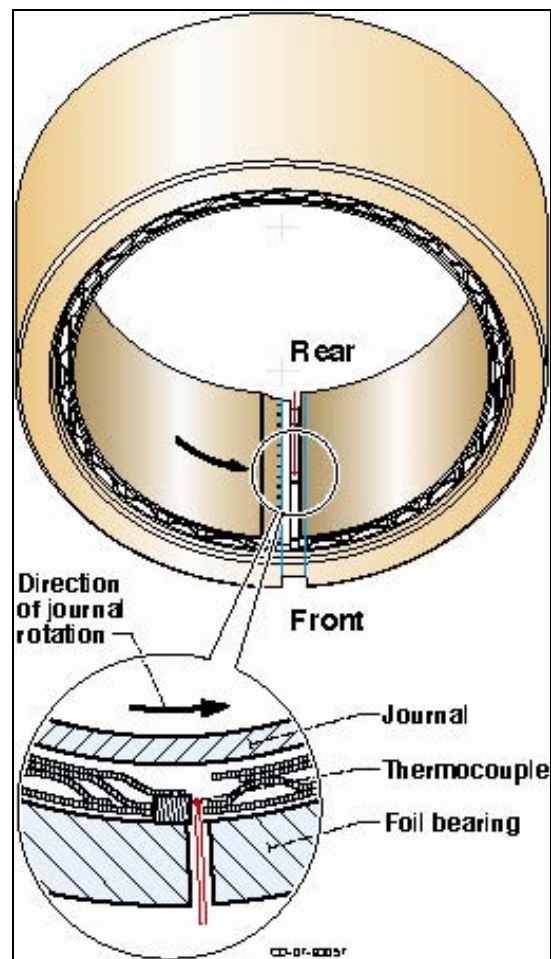

Figure 8. Drawing of the 51-mm diameter, 51-mm long
foil bearing. The type K thermocouple is located
in the middle of the bearing and on the spacer
block near the leading edge.

Figure 9. A 2-D performance map for the 51-mm diameter, 51-mm long foil bearing.

Table 2. Sample power loss data including air film temperature at the
midpoint near the leading edge for the 51-mm diameter bearing.

Speed (krpm)	Load (Newtons)	Power Loss (Watts)	Temperature (°C)
10	48	20	27
30	48	86	44
50	48	181	65
20	179	54	38
30	179	97	47
50	179	221	69

In order to prevent the onset of thermal runaway, we recommend that the bearing's operating
point always remain in its low load region from idle to maximum maneuver loads. The caveat to
this stipulation, however, is that the designer has to contend with the possible development of
excessive axial thermal gradients in the bearing. As explained in reference 18, axial thermal
gradients are postulated to arise due to the entrapment of a slug of air in the middle of the
bearing that continuously gets heated from the viscous shear, resulting in a temperature gradient
that develops across the half-width of the bearing, from the middle to the ends. Whereas thermal
runaway will result in failure, if left unchecked, the development of small thermal gradients is
not an indication of impending failure as foil bearings can safely operate in their presence.
Excessive gradients, those around 20 °C/cm or above, are a concern and can manifest during
high surface speed operation. When present, they can significantly warp the top foil to a point
that film formation is disrupted, lowering the available fluid-film for load support and leading to
high-speed rubbing contact and eventual catastrophic failure (*11*). As with thermal runaway, its
effect on the bearing is similar to a gradually increasing radial load and its progression can also
be explained via the performance map. As the gradient grows the bearing's operating point

moves vertically up from one load curve to the next and to the left since there is usually a decrease in speed due to the increased power loss. Eventually, the operating point will enter into the high load region and continue to do so until complete, and most likely catastrophic, bearing failure. This can be averted by employing an effective thermal management strategy based on maximum operating conditions to control the thermal gradient, whether by removing excess heat through indirect cooling of the journal (as was done for this research) or other effective techniques (*10*). Thermal management does not imply cooling the bearing below a certain level since high temperature operation is one of their advantages. Instead, its purpose is keep the magnitude of the temperature gradient under control to ensure the bearing's performance is not compromised while operating in the low load region of the performance map.

Thermal management can also be effective at preventing thermal runaway. This is evidenced by the existence of the power loss data in the low load region of this report, but only to a limited extent in highly preloaded bearings. Because of the steep slope of the curves in this region, off-design operation, due to a sudden, small increase in load or decrease in speed, can cause a significant jump in power loss, which could overwhelm the existing thermal management strategy, rendering it ineffective. With a passive thermal management strategy in place, the constant mass flow of air may not be sufficient to remove the extra viscous heat generated. One solution is a self-compensating system that continuously monitors the bearing's operating conditions and makes adjustments in the cooling air mass flow to counteract the excess heat. Setting up an active thermal management strategy may not only be difficult to implement but the required additional air flow will be at the expense of system efficiency. Therefore, the recommended approach is to design the system to operate only in the bearing's low load region with an acceptable margin of safety and also implement an effective thermal management strategy to prevent the formation of large axial thermal gradients.

3. Conclusions

In this report, we presented the concept of a 3-D power loss performance map as a function of speed and load. The power loss map consists of a series of individual load curves that are separated into two operating conditions, the low and high load regimes. The high load region sits on the left side of the curve's minimum point and is characterized by large changes in power loss for small variations in speed and load. Bearings designed to operate in this region are at risk of failure due to thermal runaway. Alternately, bearing's operating in the low load region on the right side of the minimum are more stable but are susceptible to the development of excessive axial thermal gradients that can lead to failure. Employing an effective thermal management strategy can control these failure modes, especially in the low load region.

As a design tool, the power loss map will compliment the load capacity and rotordynamic models during the feasibility step of the four-step process in determining the size of the bearing by forcing concessions between load capacity, stiffness, and damping and power loss. With this data, designers can then target foil air bearings that operate in their low load region throughout the system's entire operating envelope.

4. References

1. Gross, W. A. *Gas Film Lubrication*; John Wiley and Sons: New York, 1962, pp 138–114.

2. Ma, J.T.S. An Investigation of Self-Acting Foil Bearings. *ASME J. of Basic Engineering* **1965**, 837–846.

3. Barnett, M. A.; Silver, A. Application of Air Bearings to High-Speed Turbomachinery. *SAE* Paper 700720, 1970.

4. Emerson, T. P. The Application of Foil Air Bearing Turbomachinery in Aircraft Environmental Control Systems. *Proceedings of the ASME Intersociety Conference on Environmental Systems*, San Diego, CA, Paper No. 780-ENAS-18, 1978.

5. Agrawal, G. L. Foil Gas Bearings for Turbomachinery. *Proceedings of 20th Intersociety Conference on Environmental Systems*, Williamsburg, VA, SAE Paper No. 901236, 1990.

6. Lubell, D.; DellaCorte, C.; Stanford, M. K. Test Evolution and Oil-Free Engine Experience of a High Temperature Foil Air Bearing Coating. *Proceedings of GT2006: ASME Turbo Expo 2006*, Barcelona, Spain, GT2006-90572, 2006.

7. Heshmat, H.; Walton, II, J. F.; DellaCorte, C.; Valco, M. Oil-Free Turbocharger Demonstration Paves Way to Gas Turbine Engine Applications. *International Gas Turbine and Aeroengine Congress and Exhibition sponsored by ASME*, Munich, Germany, 200-GT-620, 2000.

8. Suriano, F. J. *Gas Foil Bearing Development Program*; U.S. Air Force No. AFWAL-TR-81-2095; 1981.

9. Heshmat, H.; Walton, II, J. F.; Tomaszewski, M. J. Demonstration of a Turbojet Engine Using an Air Foil Bearing," ASME Paper GT-2005-68404. *ASME Turbo Expo 2005*, Power for Land, Sea and Air, Reno-Tahoe, NV, 2005.

10. Radil, K.; DellaCorte, C.; Zeszotek, M. Thermal Management Techniques for Oil-Free Turbomachinery Systems. *STLE Tribology Transactions* **2007**, *50* (3), 319–327.

11. Dykas, B.; Howard, S. A. Journal Design Considerations for Turbomachine Shafts Supported on Foil Air Bearings. *STLE Tribology Transactions* **2004**, *47* (4), 508–516.

12. DellaCorte, C.; Radil, K. C.; Bruckner, R. J.; Howard, S. A. *A Preliminary Foil Gas Bearing Performance Map*; NASA-TM-2006-214343; 2006.

13. Salehi, M.; Swanson, E.; Heshmat, H. Thermal Features of Compliant Foil Bearings-Theory and Experiments. *ASME Journal of Tribology* **2001**, *123*, 566–571.

14. DellaCorte, C.; Valco, M. J. Load Capacity Estimation of Foil Air Journal Bearings for Oil-Free Turbomachinery Applications. *STLE Tribology Transactions* **2000**, *43* (4), 795–801.

15. DellaCorte, C. *The Effects of Substrate Material and Thermal Processing Atmosphere on the Strength of PS304: A High Temperature Solid Lubricant Coating*; NASA/TM-2002-211483; 2002.

16. DellaCorte, C. *A New Foil Air Bearing Test Rig for Use to 700 °C and 70000 rpm*; NASA/TM-107405; 1997.

17. Radil, K.; Howard, S.; Dykas, B. The Role of Radial Clearance on the Performance of Foil Air Bearings. *STLE Tribology Transactions* **2002**, *45* (4), 508–516.

18. Radil, K.; Zeszotek, M. An Experimental Investigation into the Temperature Profile of a Compliant Foil Air Bearing. *STLE Tribology Transactions* **2004**, *47* (4), 470–479.

NO. OF COPIES	ORGANIZATION
1 PDF	ADMNSTR DEFNS TECHL INFO CTR ATTN DTIC OCP 8725 JOHN J KINGMAN RD STE 0944 FT BELVOIR VA 22060-6218
1 HC	DARPA ATTN IXO S WELBY 3701 N FAIRFAX DR ARLINGTON VA 22203-1714
1 CD	OFC OF THE SECY OF DEFNS ATTN ODDRE (R&AT) THE PENTAGON WASHINGTON DC 20301-3080
1 HC	US ARMY RSRCH DEV AND ENGRG CMND ARMAMENT RSRCH DEV AND ENGRG CTR ARMAMENT ENGRG AND TECHNLGY CTR ATTN AMSRD AAR AEF T J MATTS BLDG 305 ABERDEEN PROVING GROUND MD 21005-5001
20 HCs	NASA GLENN RSRCH ATTN AMSRD ARL VT PD K RADIL (20 HCS) MS 23-2 21000 BROOKPARK RD CLEVELAND OH 44135
1 HC	PM TIMS, PROFILER (MMS-P) AN/TMQ-52 ATTN B GRIFFIES BUILDING 563 FT MONMOUTH NJ 07703
1 HC	US ARMY INFO SYS ENGRG CMND ATTN AMSEL IE TD F JENIA FT HUACHUCA AZ 85613-5300
1 HC	COMMANDER US ARMY RDECOM ATTN AMSRD AMR W C MCCORKLE 5400 FOWLER RD REDSTONE ARSENAL AL 35898-5000

NO. OF COPIES	ORGANIZATION
1 HC	US GOVERNMENT PRINT OFF DEPOSITORY RECEIVING SECTION ATTN MAIL STOP IDAD J TATE 732 NORTH CAPITOL ST NW WASHINGTON DC 20402
1 HC	US ARMY RSRCH LAB ATTN AMSRD ARL CI OK TP TECHL LIB T LANDFRIED BLDG 4600 ABERDEEN PROVING GROUND MD 21005-5066
1 HC	DIRECTOR US ARMY RSRCH LAB ATTN AMSRD ARL RO EV W D BACH PO BOX 12211 RESEARCH TRIANGLE PARK NC 27709
3 HCS	US ARMY RSRCH LAB ATTN AMSRD ARL CI OK PE TECHL PUB ATTN AMSRD ARL CI OK TL TECHL LIB ATTN IMNE ALC HRR MAIL & RECORDS MGMT ADELPHI MD 20783-1197

TOTAL: 33 (1 PDF, 1 CD, 31 HCs)